THE JOURNAL OF PHYSICAL CHEMISTRY A
A JOURNAL OF THE AMERICAN CHEMICAL SOCIETY

pubs.acs.org/JPCA

Article

Quantification of the Helicality of Helical Molecular Orbitals

Published as part of The Journal of Physical Chemistry virtual special issue "125 Years of The Journal of Physical Chemistry".

William Bro-Jørgensen, Marc H. Garner, and Gemma C. Solomon*

Cite This: *J. Phys. Chem. A* 2021, 125, 8107–8115

Read Online

ACCESS | Metrics & More | Article Recommendations | Supporting Information

ABSTRACT: The frontier molecular orbital (MO) topology of linear carbon molecules, such as polyynes, can be visually identified as helices. However, there is no clear way to quantify the helical curvature of these π-MOs, and it is thus challenging to quantify correlations between the helical curvature and molecular properties. In this paper, we develop a method that enables us to compute the helical curvature of MOs based on their nodal planes. Using this method, we define a robust way of quantifying the helical nature of MOs (helicality) by their deviation from a perfect helix. We explore several limiting cases, including polyynes, metallacumulenes, cyclic allenes, and spiroconjugated systems, where the change in helical curvature is subtle yet clearly highlighted with this method. For example, we show that strain only has a minor effect on the helicality of the frontier orbitals of cycloallenes and that the MOs of spiroconjugated systems are close to perfect helices around the spiro-carbon. Our work provides a well-defined method for assessing orbital helicality beyond visual inspection of MO isosurfaces, thus paving the way for future studies of how the helicality of π-MOs affects molecular properties.

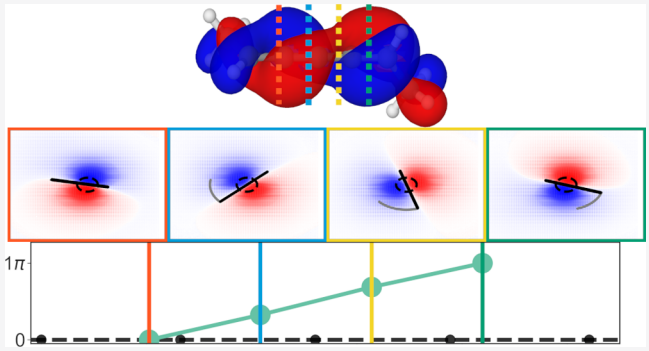

INTRODUCTION

Molecular orbitals (MOs) have long been an essential tool in the toolbox of chemists. While they are not physical observables, they have nonetheless been used to develop intuition for and predict physical properties.[1−5] Recently, the π-MOs of some linear carbon molecules have received increased attention due to their helical topology.[6−17] An example of such a proclaimed helical π-orbital is shown in Figure 1. This is the HOMO of *S*-1,5-Me-[4]cumulene, and it is clearly shaped like a helix. In appropriately substituted molecules, these MOs occur due to mixing of the otherwise orthogonal π-systems as the symmetry of the molecule is reduced.[15] This helical nature of the π-system is a fundamental consequence of the molecular symmetry and is evident when an appropriate Hückel model is made for the symmetry-adapted MOs as shown in Figure 1b. Even at the Hückel level of theory, it is clear that the MOs are imperfect helices as the angular steps along the molecular axis differ in magnitude.[15] The *helicality* of the electronic structure is thus ill-defined as even the most helical cases may not be perfect cylindrical helices. In the following, we will use the term "helicality" to refer to how close an MO is to a cylindrical helix. The helicality of an MO is large if it is close to a perfect cylindrical helix.

Given the interest in helical MOs as a means to understand related properties and the range of molecular systems in which these MOs appear,[18−33] it is problematic that the assessment of helical MOs relies on visual inspection alone. It is thus altogether binary; if an MO is shaped like a coil, we may deem it to be helical. This definition suffices to classify the trivial example shown in Figure 1a because we can clearly see that the MO is shaped like a helix. However, we need a more stringent definition if we wish to deal with cases of varying degrees of helicality. Without a quantifiable measure of the degree of helicality of the MOs, it will not be possible to directly correlate them with observable molecular properties.

A helix is a mathematically well-defined construct. In Cartesian coordinates, a cylindrical helix, as shown in Figure 1c, is defined by the following equations:

$$\begin{aligned} X(\phi) &= r\cos(\phi) \\ Y(\phi) &= r\sin(\phi) \\ Z(\phi) &= h\phi \\ \text{pitch} &= 2\pi h \end{aligned} \tag{1}$$

Received: June 30, 2021
Revised: August 23, 2021
Published: September 7, 2021

https://doi.org/10.1021/acs.jpca.1c05799
J. Phys. Chem. A 2021, 125, 8107–8115

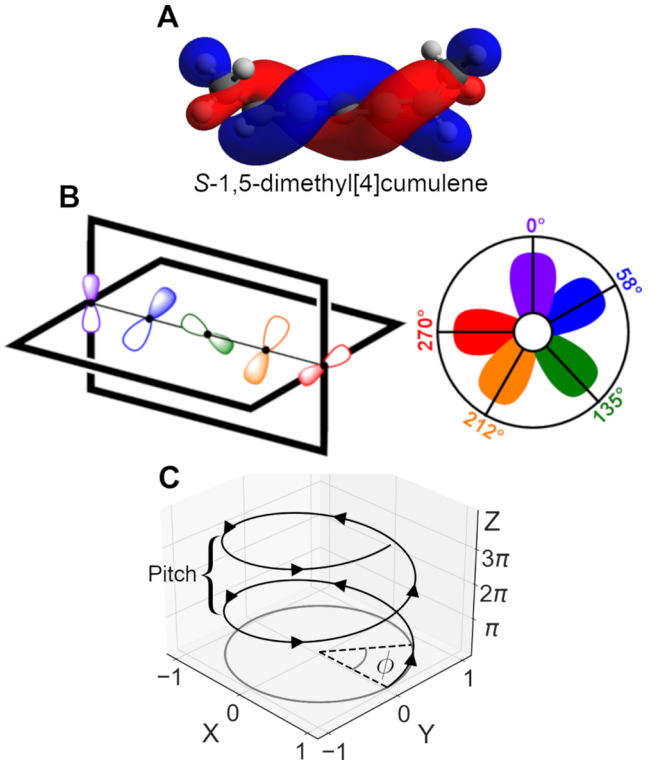

Figure 1. Illustration of helical MOs from DFT and Hückel theory and a cylindrical helix. (A) The highest occupied MO (HOMO) from a DFT calculation on *S*-1,5-Me-[4]cumulene. (B) Illustration of the HOMO from a Hückel calculation on [4]cumulene. On the left, each atomic orbital is plotted along the carbon chain and colored by an atom site (from violet to red). On the right, a diagrammatic representation of the twist angles of the MOs projected along the *z*-axis. For clarity, we have only plotted the positives lobes. Adapted with permission from ref 15. (C) A right-handed helix from $\phi = 0$ to 3π with $r = 1$. The mathematical definition is given beneath the plot.

Here, r is the radius of the helix and h is a parameter describing the vertical separation between each loop of the helix that is related to the pitch. The angle ϕ is defined as shown in Figure 1c. A cylindrical helix is a curve that forms a constant angle with respect to the axis of the cylinder. Intrinsic to this definition, it has constant nonzero curvature and constant nonzero torsion. Curvature and torsion are defined by

$$\kappa = \frac{1}{R} = \frac{r}{r^2 + h^2} \tag{2}$$

Here, R is the radius of curvature and κ is the curvature. A curve with zero curvature is a straight line. The sign of κ determines which way the helix turns with positive curvature being a right-handed (P) helix and negative curvature a left-handed (M) helix. Intuitively, curvature can be understood as to how big a cylinder the helix encloses: large curvature translates to a cylinder with a small radius. The torsion of the helix, τ, is defined as

$$\tau = \frac{h^2}{r^2 + h^2} \tag{3}$$

A positive τ gives a helix with twist up the z-axis while a negative τ gives twist down the z-axis. Torsion can intuitively be understood as to how drawn out or compressed the helix is. A helix with high torsion will have a large pitch so that a large increase in z occurs when a full turn is completed. A helix with no torsion will be a circle with curvature of $1/r$. It is thus possible to define objects with perfect helicality (perfect helices) and use this for assessing the helicality of less helical objects. We refer to O'Neill for a more general mathematical derivation.[34]

In this work, we define a mathematically rigid method for assessing how helical an MO is. We use this method, which we will refer to as the quantification of helicality (QoH) method, to assess several limiting cases in the form of substituted [n]cumulenes, polyynes, metallacumulenes, and spiroconjugated molecules. The article proceeds as follows. We go through four different examples that showcase the diversity of systems where helical MOs arise. First, we reassess *S*-1,9-Me-[8]cumulene and 1,1-Me-[8]cumulene where the MO helicality is visually apparent. Next, we show examples where the helicality of the HOMO changes when the end-groups of 1,4-diphenyldiyne and *trans*-1,6-Me-[5]cumulene are twisted. We examine the helical MOs in *trans*-[EtC═(C═)$_4$C═Ru═(C═)$_4$CMe]$^{2+}$, a metallacumulene with a ruthenium atom in between two cumulenylidene ligands. After that, we go through the MOs of spiropentadiene and spirononatetraene, a slightly different class of compounds compared with cumulenes that still exhibit helical MOs. Finally, we assess the MOs in cycloallenes with a ring size of up to 9. Our analysis of these systems establish the varying degrees of helicality that is not apparent from a visual inspection of the MOs.

METHODS

Molecules were optimized in the gas phase by using Gaussian16 with density functional theory (DFT) using the Perdew–Burke–Ernzerhof (PBE) exchange-correlation functional.[35] The 6-311G(d,p)basis set was used for all atoms. The optimization threshold was set to *tight*, and an *ultrafine* integral grid was used. MOs are plotted at an isosurface value of 0.02 unless otherwise noted. For the metallacumulene, we used the cc-pVTZ basis set for C, H, and P[36,37] atoms and the SDD basis set and effective core potential for the Ru atom.[38]

To quantify how helical an MO is, we first need to define the component of the MO that we want to consider. A helical MO has two defining characteristics: Its nodal plane propagates helically through space and so will any choice of isovalue (a specific value of the wave function amplitude).[15] While this allows for two different approaches for defining helicality, we choose the spatial propagation of the nodal plane along the molecular axis. In the Supporting Information, we provide a description of how to evaluate an MO on a real-space 3D grid. We also provide another way of quantifying helicality by fitting the equation for a helix to the highest isovalue along the carbon chain. We use the spatial propagation of the nodal plane in the following because it is conceptually simpler and more robust in less well-defined helical systems.

In Figure 2A, we outline the workflow of our method. After generation of a .cube file, we slice the MO into *xy*-planes along the *z*-axis (the molecular axis of the carbon chain). The increment between each slice will correspond to the resolution chosen when evaluating the MO on a real-space grid. In all our examples, we have 1/12 bohr = 44 mÅ between each slice. In the following example, we use the HOMO of 1,5-diMe-[4]cumulene shown in Figure 2B. For each slice, we only keep a subset of MO amplitude data points by filtering out any point that lies more than x Å away from (0, 0). In most cases, reasonable choices of x lie between 0.5 and 1.0 Å. After filtering, we locate all the places where the MO amplitude

https://doi.org/10.1021/acs.jpca.1c05799
J. Phys. Chem. A 2021, 125, 8107−8115

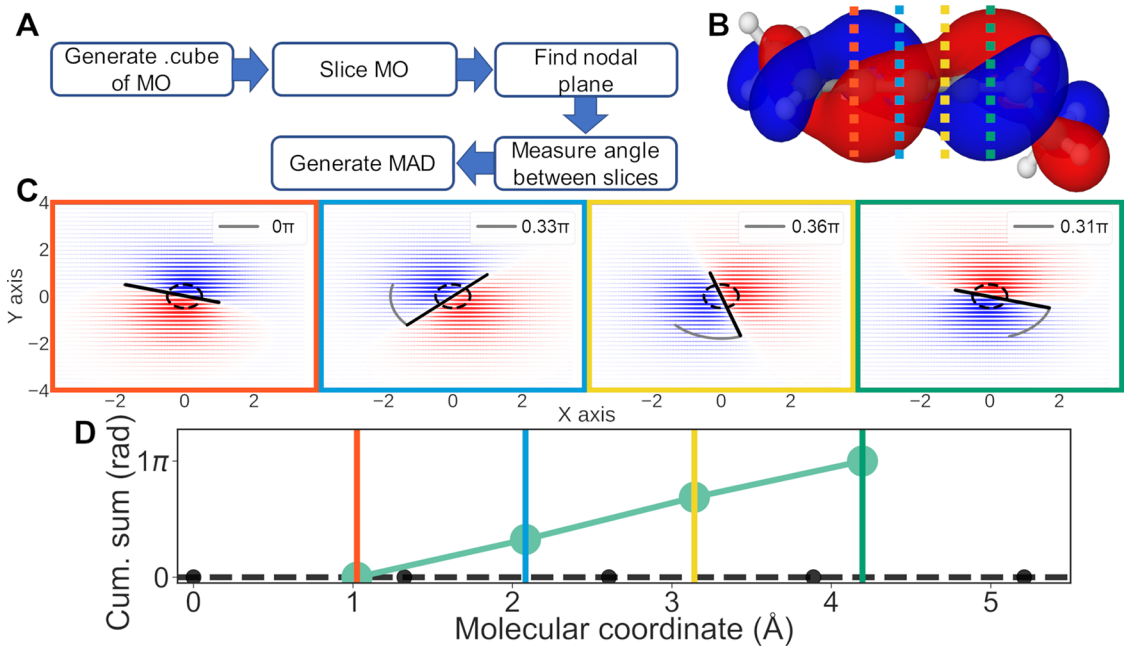

Figure 2. Illustration of the QoH method. (A) Workflow of our method. (B) HOMO of *S*-1,5-Me-[4]cumulene with colored lines showing the locations where the slices in the bottom are extracted from. (C) Slices in the *xy*-plane (*z*-axis along carbon chain) of the HOMO shown at the top. The size of each dot corresponds to the MO amplitude at each point in space, while red and blue denotes the sign (red: positive; blue: negative). The black line is a fitted, straight line through the points where the MO changes sign. The gray line denotes the angle between the given slice and the previous slice. The legend provides the change in angle in fractions of π. The procedure is explained in depth in the Supporting Information.

changes sign; that is, we find the π-nodal plane. This gives two lists of points: one with points found before reaching zero (list **A**) and one with points found after a zero (list **B**). A new set of points is calculated (list **C**) as the midpoint between the corresponding points in **A** and **B**. **C** thus contains the approximated points in space where the MO phase changes. The points of **C** are then fitted to a straight line where the offset has been fixed to 0. This is the black line seen in the four panels of Figure 2C. This black line is a systematic representation of the π nodal plane in each slice, which we can use to visualize the nodal plane of a given MO. We can determine the angle between two subsequent slices by using arctan2 as defined in NumPy.[39] We use this to measure the angular propagation of the MO nodal plane through the molecule. In Figure 2C, the angular propagation between each slice is illustrated by the gray line and given as fractions of π in the legend. By taking the cumulated sum of all the angles in **C**, we can compare the helicality of MOs in different molecules quantitatively. The cumulated sum is shown in Figure 2D. The code to find the nodal plane of an arbitrary, helical MO and calculate the helicality throughout the MO has been uploaded to Github alongside a short description of usage. It is available at https://github.com/chem-william/find_nodal.

In the Introduction, we defined a cylindrical helix as a curve that forms a constant angle with respect to the axis of a cylinder. A constant increase in twist between successive slices of the nodal plane is thus the principal defining feature of a cylindrical helix. From this, we expect that the cumulated sum of the angles between successive slices will be a straight line. Any deviation from a straight line indicates deviation from a perfect helix. By quantifying how much a straight line fit deviates from the cumulated sum of angles, we can find how much the MO deviates from a perfect helix. As a quantitative summary of how much a given MO deviate from a perfect helix, we report the mean absolute deviation (MAD). A higher MAD indicates deviation from a perfect helix, and a lower MAD indicates that the MO is closer to a perfect helix. This deviation thus provides a rigid measure of the helicality. The MAD is given by

$$\mathrm{MAD} = \frac{1}{n}\sum_{i=1}^{n} |y_i - f_i| \tag{4}$$

where n is the number of data points, y_i is each observed data point, and f_i is each data point predicted by the fitted straight line.

RESULTS

Substituted odd-carbon cumulenes constitute the clearest example of the difference between helical and rectilinear π-MOs in linear molecules. To provide examples of the potential of the QoH method, we start by revisiting longer cases than those discussed in the Introduction. In Figure 3, we assess the HOMO of achiral 1,1-Me-[8]cumulene and chiral *S*-1,9-Me-[8]cumulene. The former is a clear case of a rectilinear HOMO and the latter of a helical HOMO. In the graph of the cumulated sum, we see that the rectilinear HOMO of 1,1-Me-[8]cumulene increases with a series of steps. Its cumulated sum of the twist does not change at all for the first ∼2 Å and then makes an abrupt jump of π rad (180°) when there is a node in the MO. The HOMO of *S*-1,9-Me-[8]cumulene has an almost constant increase in the cumulated sum, and as explained in Methods section, this is one of the defining features of a cylindrical helix. The MAD for the helical MO is 6, which gives an indication of a "low" value that suggests an almost perfect helix. In comparison, the MAD of the rectilinear HOMO of 1,1-Me-[8]cumulene is 51.

The MAD captures what we intuitively expect from a visual inspection of the isosurfaces: the HOMO is a cylindrical helix

https://doi.org/10.1021/acs.jpca.1c05799
J. Phys. Chem. A 2021, 125, 8107−8115

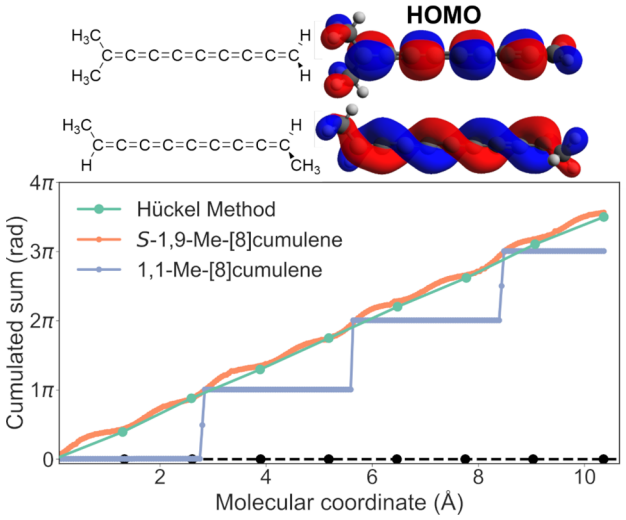

Figure 3. Change in helicity for three different systems. (top) Chemical structures and HOMO of 1,1-Me-[8]cumulene and *S*-1,9-Me-[8]cumulene, respectively. (bottom) The cumulated sum of the twist of the HOMO plotted against length along the cumulenic axis of the Hückel method, 1,1-Me-[8]cumulene, and *S*-1,9-Me-[8]-cumulene. The black, filled circles indicate the position of the carbon atoms along the carbon chain of *S*-1,9-Me-[8]cumulene, and the black, dashed line is a guide to the eye. The carbon positions of both systems are nearly identical; therefore, only one carbon chain is depicted. Isovalue 0.02 au.

in one case and nonhelical in the other. It is worth noting here that the MAD has no upper limit for the rectilinear HOMO. Only the case of a perfect cylindrical helix is well-defined by this method, and the rectilinear shape of an MO is thus a case that is classified as *not* a cylindrical helix.

The QoH method also allows us to carry out the analysis by using the Hückel model of an [8]cumulene where the appropriate C_2 symmetry has been enforced (see the Supporting Information).[15] As is clear from Figure 3, there is good correspondence between the results from the Hückel model and the helical MO of *S*-1,9-Me-[8]cumulene found by using DFT. In the Hückel model, there is again a slight deviation from perfect helicality with a MAD of 3. For the Hückel model, there are only nine sites, one for each carbon atom. This means that we only have nine data points in the graph of Figure 3 whereas the DFT-MOs are evaluated on a near-continuous 3D grid. The agreement found here between Hückel theory and higher-level calculations shows the underlying commonalities in these two descriptions of the π-MOs. In the remaining sections, we will focus on assessing molecules where the orbital helicality is less clear than in this initial example.

Polyynes. Polyynes are linear chains of sp-hybridized carbon that can exhibit helical MOs visually similar to those seen in α,ω-substituted even [n]cumulenes.[10−13,20,21,26,27] Similarly, odd [n]cumulenes can also exhibit helical MOs when the end-groups are rotated away from a coplanar orientation as we show at the top of Figure 4. There is almost free rotation for the end-groups of polyynes with the ground-state orientation determined by the type of end-groups.[40−44] The ground state of odd [n]cumulenes is the coplanar geometry, and there are considerable barriers to torsion.[27,45−49] Because the ground state for both molecules converges to coplanar end-groups, all MOs for structures with a dihedral angle >0° are single-point calculations where the dihedral angle has been set manually with the remaining internal degrees of freedom frozen. Note that to avoid confusion, we systematically use degrees for the torsion angles

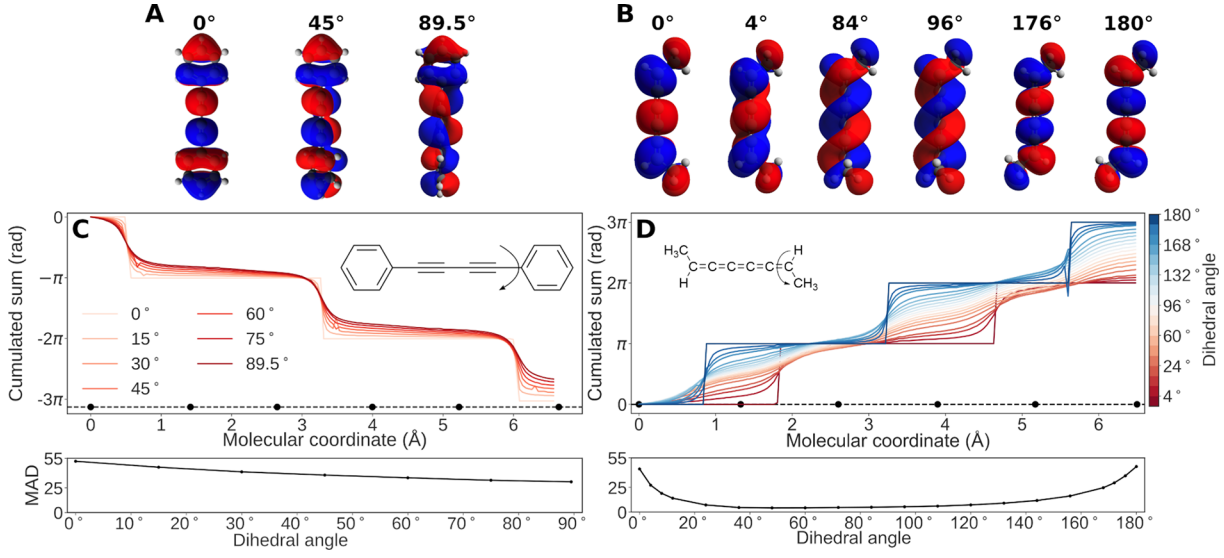

Figure 4. Change of the HOMO of diphenyl-diyne and *trans*-1,6-Me-[5]cumulene with increasing torsion angle. (A) HOMO of diphenyl-diyne at 0°, 45°, and ∼90° dihedral angles. Note that the dihedral angle in the final is calculated at 89.5° to break the symmetry. (B) HOMO (first three) and LUMO (last three) of *trans*-1,6-Me-[5]cumulene at 0°, 4°, 84°, 96°, 176°, and 180° dihedral angles. (C) The cumulated sum of the twist of the HOMO of diphenyl-diene plotted against length along the polyynic axis at different dihedral angles. (D) The cumulated sum of the twist of the HOMO of *trans*-1,6-Me-[5]cumulene plotted against the length along the cumulenic axis at different dihedral angles. Below each plot, the MAD is plotted for a straight line fit through the cumulated sum of angles at each dihedral angle. The filled circles indicate the position of the carbon atoms along the carbon chain. Note that we systematically use degrees for the torsion angles of the end-groups, whereas radians are used to denote the helical twist of the MOs. Isovalue: 0.01 au.

https://doi.org/10.1021/acs.jpca.1c05799
J. Phys. Chem. A 2021, 125, 8107−8115

of the end-groups, whereas radians are used to denote the helical twist of the MOs.

Starting with the diphenyl-diyne, at the top left of Figure 4, we show its HOMO at three different dihedral angles of the end-groups. For the molecule to retain C_2 symmetry, the final step of twisting is at 89.5° instead of at 90°. If we were to rank the three HOMOs shown in terms of their helicality on the basis of visual inspection, it is clear that the 0° case is the least helical. However, we cannot easily distinguish whether the end-group at 45° or 89.5° leads to the most helical MOs or if the helicality is perhaps equal. The analysis of the cumulated sum of angles provides a quantitative answer to this problem. When the dihedral angle of the end-group is 0°, the cumulated sum of angles increases with a series of steps as we expect from a rectilinear MO. By increasing the dihedral angle of the end-groups, the cumulated sum of twist through the HOMO gradually becomes less staircase-like. Instead, it approaches the constant increase we associate with a helix. We see that increasing the dihedral angle of the end-group correlates systematically with a decrease in the MAD. Therefore, we can quantitatively say that an increase in the torsion angle gives an increase in helicality. This analysis also reveals that the HOMO does not achieve perfect helicality; instead, the increase in helicality saturates with a MAD ∼ 30 as we approach a dihedral angle of 90°.

The analysis for the similar 1,6-Me-[5]cumulene is shown on the right in Figure 4. At the top right of Figure 4, we show the HOMO at six different dihedral angles for the [5]-cumulene. At 0° and 180°, the π-orbitals have a rectilinear shape as the two π-orbital systems in the molecule are separated due to the D_{2h} symmetry and the MO results from contributions from only one of the π-systems. Starting from 0°, as the dihedral angle between the end-groups increases, the HOMO−LUMO gap narrows, and at 90° the HOMO and LUMO become degenerate and cross.[27] With increasing dihedral angle, we again see an increase in the helicality of the HOMO that saturates close to 90° and then decreases again with a further increase toward 180°. There is a notable difference from the diphenyl-diyne. The helicality increases quickly with twist, reaching a MAD < 10 already at a 20° dihedral angle, and then slowly decreases to a minimum MAD of 4. Thus, the HOMO becomes an almost perfect helix much like the odd-carbon cumulene.

The MAD thus allows for a direct comparison of the helicality of different molecules. Comparing the ∼90° cases for both molecules, it is clear that the HOMOs of the [5]- and [8]cumulenes are closer to a cylindrical helix than that of the diphenyl-diyne. This underlines that MO helicality is not just a property of the torsion angle but depends on the chemistry of the end-groups that ultimately controls if a linear carbon chain is cumulenic or polyynic.[50] This lack of perfect helicality may be linked to the more significant bond-length alternation in the diyne. We observe the maximal twist at the single bonds as this is where the occupied frontier MOs are antibonding.

Metallacumulenes. Metallacumulenes and -ynes are another class of molecules that may exhibit helical MOs in the linear fragments of the molecules.[16,51−53] Synthesis of long [n]cumulenes poses a practical challenge because they are rather unstable.[54] However, by complexing the cumulenes with a transition metal, the reactivity of the cumulenylidene ligands can be brought down due to both electronic and steric effects.[55−59] Since the first organometallic compounds with cumulene moieties were reported by Fischer et al.[60] and Berke,[61] the synthesis of complexes with great structural variation continues to be an active field.[62−67] Formally, the metallacumulene shown in Figure 5 has C_1 symmetry, and any

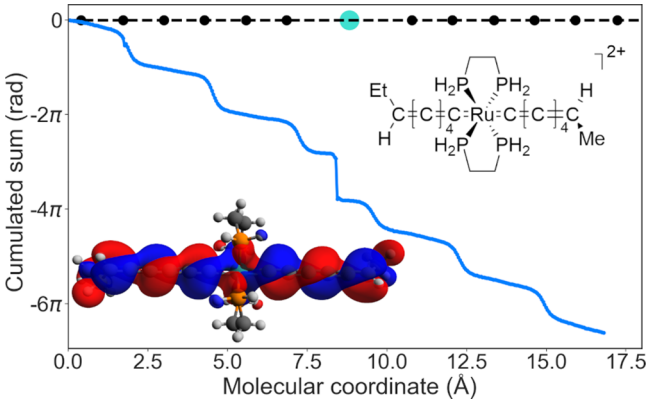

Figure 5. Cumulated sum of the twist of the HOMO plotted against length along the cumulenic axis of *trans*-[EtC═(C═)$_4$C═Ru═(C═)$_4$CMe]$^{2+}$. The chemical structure is shown in the upper right, and its HOMO is shown in the lower left of the plot. The filled circles indicate the position of atoms along the cumulenic carbon chain (black: carbon; turquoise: ruthenium), and the black, dashed line is a guide to the eye.

MO helicality will therefore not be symmetry-protected. Note that the metallacumulene illustrated in Figure 3 has had the phenyl groups replaced with hydrogens to speed up calculations. From the HOMO illustrated in the bottom of Figure 5, it is clear that this MO is somewhat helical. Still, visual assessment of the helicality of this MO compared with the previous MOs is challenging. Again, we plot the cumulated sum of angles through the entire molecule (blue curve in Figure 5). This helical MO deviates from a cylindrical helix as it exhibits the rounded step-like line shape that we saw previously. We can also see that at the ruthenium center there is a jump in the evolution of the helical MO of approximately π radians. This jump is due to the inherent sign change in the metal d-orbitals that couple to the carbon p-orbitals. As we also saw in the previous example, the cumulated sum along the chain provides us with a richer understanding of how the helicality changes compared with visual inspection of the MO.

Because of the jump of π radians in the cumulated sum at the ruthenium, there are two different ways of summarizing how much the HOMO deviates from a cylindrical helix. It is possible to make a straight line fit to all the data points or, alternatively, to split the points into two sets, comprising points before or after the ruthenium where there is an inherent deviation from perfect helicality. The resulting MAD for these approaches is shown in Table 1.

Table 1. MAD for Line Fits to the Data Shown in Figure 5

	MAD
total[a]	40
before Ru[b]	22
after Ru[b]	18
mean[c]	20

[a]Fit of the whole data set. [b]Fit of only the data before or after Ru. [c]Mean of the MAD before and after Ru.

https://doi.org/10.1021/acs.jpca.1c05799
J. Phys. Chem. A 2021, 125, 8107−8115

Comparing the two measures for the total helicality (entries "total" and "mean" in Table 1), we see that independent of which approach we choose, both suggest that the HOMO of the metallacumulene shown in Figure 5 deviates more from a cylindrical helix than the HOMO of *S*-1,9-Me-[8]cumulene; still, in the individual cumulenic parts the deviation is less than that in the polyynes. Comparing the MAD for the fit of the data before and after the ruthenium center ("before Ru" and "after Ru" entries in Table 1), we see that both parts have similar MAD, suggesting that the helicality of both sides of the metallacumulene are comparable. This might not be the case for other types of metallacumulenes with a different choice of substituents. The possibility of variable helicality in different parts of a single molecule means that metallacumulenes may make it possible to test how different molecular properties correlate with helicality in separate molecular components (here the ligands). It provides an interesting testbed as many other molecular properties would be kept constant, isolating the impact of helical MOs.

Spiroconjugated Molecules. Next, we examine the simple spiroconjugated molecules 1,6-dimethylspiro[4.4]-nonatetraene and 1,4-dimethylspiro[2.2]pentadiene.[68−71] As with the even [*n*]cumulenes, metallacumulenes, and polyynes, the two orthogonal π-systems may interact and mix.[72,73] However, only half of the frontier MOs of spiroconjugated molecules become helical when the molecules are appropriately substituted.[30] As the helicality of their MOs might influence optical properties,[30] the quantification of helicality is of interest. The carbon chain is defined as the carbon atoms in the shortest through-bond path between the methyl groups. Note that the distance between the solid circles in Figure 6 (symbolizing carbon atoms) is the bond distance between two adjacent carbons and not the *z*-coordinate for each carbon.

Starting with the HOMO−2 and HOMO−3 of dimethylspiro[4.4]nonatetraene (blue and red at the top of Figure 6), we see nonuniform helicality across the molecule. There is a linear increase/decrease evident in the cumulated sum across the center of the molecule, indicating helical orbitals, versus steplike behavior close to the methyl groups. This is hard to see by visual inspection of the MOs in the top left corner of Figure 6. Furthest away from the spiro-carbon the orbitals are more similar to the rectilinear MOs we see in the unsubstituted spiro[4.4]nonatetraene or, simply, cyclopentadiene (see Figure S3). This is also reflected in the MAD shown in Table 2: Using the full data set gives a MAD of 17 for both HOMO−2 and 18 for HOMO−3. On the other hand, if the data set is limited to the carbons directly adjacent to the spiro-carbon, we get a MAD of 3 for the HOMO−2 and 8 for the HOMO−3. These two MAD also suggest that there is a quantifiable difference in helicality between the HOMO−2 and HOMO−3. This difference is again not clear from the isosurface plotted at the top of Figure 6 but is noticeable in the graph of the cumulated sum. For spiro[2.2]pentadiene (bottom of Figure 6), the angular twist of the HOMO and HOMO−1 increases/decreases almost linearly. This is apparent from both the cumulated sum and the MAD (see Table 2), which is very close to 1. For both molecules, their MOs hardly deviate from a cylindrical helix when close to the spiro-carbons, and consequently, both sets of MOs are similar to each other in this region. Moving away from the spiro-carbon, the dimethylspiro[4.4]nonatetraene starts to resemble a rectilinear π-MO whereas the helical character persists in the HOMO and HOMO−1 of dimethylspiro[2.2]pentadiene.

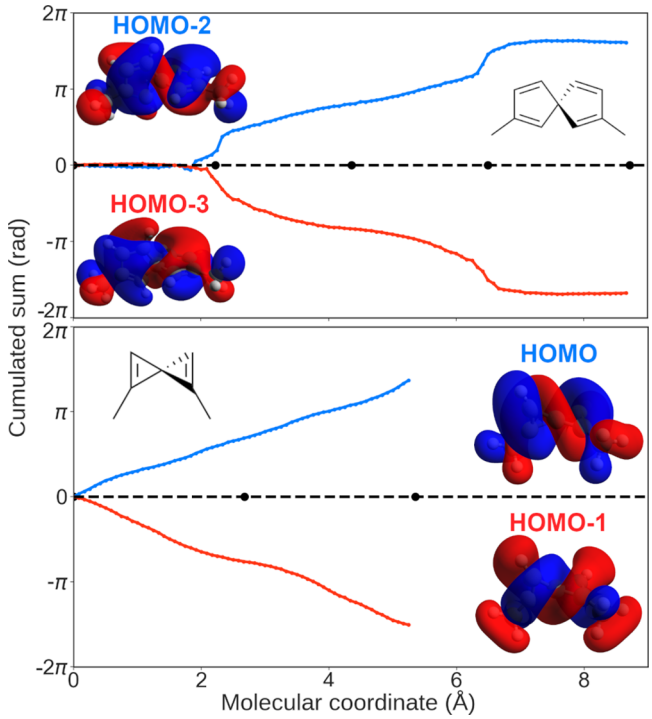

Figure 6. Cumulated sum of the twist of the MO twist plotted against length along the molecular axis of dimethylspiro[4.4]nonatetraene (top) and dimethylspiro[2.2]pentadiene (bottom) for selected pairs of orbitals shown in blue and red. The molecular axis is defined as the shortest through-bond path between the two methyl groups. Chemical structures of the two molecules are shown to the right in the top graph and to the left in the bottom graph. The highest occupied MO pairs and helical MO pairs of each molecule are shown opposite to the chemical structures. The black filled circles indicate the position of the carbon atoms along the designated carbon chain, and the black dashed line is a guide to the eye. Isovalue: 0.01 au.

Table 2. MAD for Line Fits to the Data Shown in Figure 6

	MAD
dimethylspiro[4.4]nonatetraene (5 carbons)[a]	
HOMO−2	17
HOMO−3	18
dimethylspiro[4.4]nonatetraene (3 carbons)[a]	
HOMO−2	3
HOMO−3	8
dimethylspiro[2.2]pentadiene	
HOMO	2
HOMO−1	7

[a]Refers to length of the carbon chain across the spiro-carbon included in the fit.

Cycloallenes. Finally, we examine cyclic allenes where the allenic moiety is constrained, thus perturbing the helical π-system. Cycloallenes are synthetically interesting compounds that, given their reduced symmetry due to the ring structure, exhibit helical MOs.[30,31,74−79] Most recently, Ramirez et al.[31] demonstrated that secondary orbital interactions due to the helical frontier MO topology are responsible for the *endo* selectivity in Diels−Alder reactions. Four molecular structures of simple cycloallenes are shown in the top of Figure 7, from left to right: 1,2-cyclohexadiene, 1,2-cycloheptadiene, 1,2-cyclooctadiene, and 1,2-cyclononadiene. Unlike the linear carbon chain in allene, cycloallenes are strained compounds

https://doi.org/10.1021/acs.jpca.1c05799
J. Phys. Chem. A 2021, 125, 8107−8115

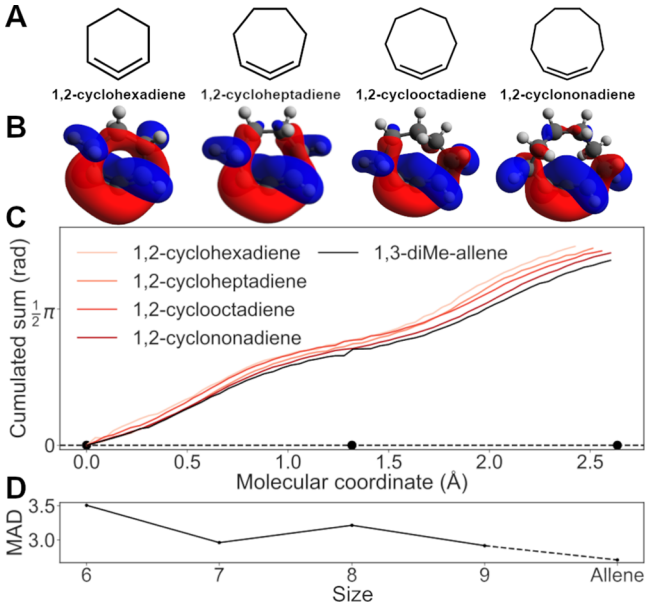

Figure 7. Change of the HOMO in four different cycloallenes with increasing ring size. (A) Chemical structure of 1,2-cyclohexadiene, 1,2-cycloheptadiene, 1,2-cyclooctadiene, and 1,2-cyclononadiene. (B) HOMO for each of the cycloallenes. (C) The cumulated sum of the twist of the HOMO plotted against length along the allenic chain. The black filled circles indicate the mean allenic carbon positions across the four molecules. (D) MAD for all four cycloallenes. The black dashed line is a guide to the eye.

where the two cumulated double bonds sit at a slightly bent angle relative to each other. This angle approaches 180° with increasing ring size and will thus eventually be close to 1,3-dimethylallene.[80]

The HOMO for each of the four cycloallenes is shown in Figure 7. While it is visually clear that these four MOs are helical, it is not clear how their helicality ranks relative to each other. Looking at the cumulated sum of twist along the carbon chain, we can see that the helicalities of all four MOs are similar and follow the same trend. All four have an almost linear increase of the cumulated sum with a slight flattening close to the allenic carbon. This also means that all four have a high degree of helicality with a MAD below 3.5, as seen in the bottom plot of Figure 7. Comparing the helicalities of the four cycloallenes with that of 1,3-diMe-allene, we see that the helicality of the cycloallenes approaches the helicality of the 1,3-diMe-allene with increasing ring size as expected. The bending of the cumulated double bonds introduced by the ring has only a minimal effect on the helicality. The introduction of cyclic substituents further enables the fine-tuning of the helical MOs without destroying helicality.

CONCLUSIONS

In this work, we have developed a method that can determine how the helical twist of π-MOs evolves through any given molecule. This method can be used to quantify the deviation of the MO from a perfect cylindrical helix and thus allows us to probe the helicality of MOs for a diverse set of molecules. We find a pronounced difference in the change in helical curvature of the π-MOs of different types of linear systems. Notably, the MOs of polyynes do not achieve the same level of helicality as equivalent-length cumulenes. The distribution of helical twist of the MOs depends on the chemical nature of the π-system. This change in uniformity of the twist is not tied to the difference between polyynic and cumulenic systems as the staircase-like features, and this change in helicality, are also present in the investigated metallacumulene, *trans*-$[EtC{=}(C{=})_4C{=}Ru{=}(C{=})_4CMe]^{2+}$. The degree of helicality is very sensitive to some types of structural changes while being almost invariant to other types. For example, twisting the end-groups of polyynes and cumulenes has a considerable effect on the helicality of their MOs. Contrarily, the bent bond angles in cycloallenes has a negligible effect on the helicality of their HOMO. Our method allows for a straightforward and systematic analysis of a range of molecular systems independent of how each system is partitioned.

Going forward, the development of tools for systematical quantification of helicality in MOs is a prerequisite to investigate how helical MOs correlate with or can be used to predict, molecular properties. This might, for example, allow us to control molecular properties based on our knowledge of how to chemically manipulate helical MOs. As we become increasingly aware of molecules where helical π-systems appear, the need grows for better tools to make quantitative assessments of helicality. In this work we have used MAD as the quantitative descriptor of orbital helicality because it both summarizes how well the data follow a given model and allows for comparison across data sets. While there may be more elaborate measures that could be envisaged, it is a simple, intuitive, and well-known assessment approach. The use of MAD as the test for cylindrical helicality answers the following question: Is the MO a perfect helix or not? While the case of a cylindrical helix is well-defined and corresponds to a MAD of 1, the "or not" situation is less well-defined as there will be more situations that deviate from a cylindrical helix. In practice, this is not a problem in this study. However, future work may aim for a more distinct definition of the edge cases, especially if MO helicality turns out to be decisive for molecular properties.

ASSOCIATED CONTENT

Supporting Information

The Supporting Information is available free of charge at https://pubs.acs.org/doi/10.1021/acs.jpca.1c05799.

Information on how to access all analyzed molecular structures; description of workflow; Hückel model for [8]cumulene; benchmark of functionals and basis sets; helical propagation of isovalues; molecular orbitals of cyclopentadiene (PDF)

AUTHOR INFORMATION

Corresponding Author

Gemma C. Solomon − *Department of Chemistry and Nano-Science Center, University of Copenhagen, DK-2100 Copenhagen Ø, Denmark;* orcid.org/0000-0002-2018-1529; Email: gsolomon@chem.ku.dk

Authors

William Bro-Jørgensen − *Department of Chemistry and Nano-Science Center, University of Copenhagen, DK-2100 Copenhagen Ø, Denmark;* orcid.org/0000-0001-8171-6374

Marc H. Garner − *Department of Chemistry and Nano-Science Center, University of Copenhagen, DK-2100*

https://doi.org/10.1021/acs.jpca.1c05799
J. Phys. Chem. A 2021, 125, 8107−8115

Copenhagen Ø, Denmark; orcid.org/0000-0002-7270-8353

Complete contact information is available at: https://pubs.acs.org/10.1021/acs.jpca.1c05799

Notes

The authors declare no competing financial interest.

■ ACKNOWLEDGMENTS

This project has received funding from the European Research Council (ERC) under the European Union's Horizon 2020 research and innovation programme (Grant Agreement No. 865870).

■ REFERENCES

(1) Griffith, J. S.; Orgel, L. E. Ligand-field theory. *Q. Rev., Chem. Soc.* **1957**, *11*, 381−393.
(2) Woodward, R. B.; Hoffmann, R. The Conservation of Orbital Symmetry. *Angew. Chem., Int. Ed. Engl.* **1969**, *8*, 781−853.
(3) Zimmerman, H. E. Moebius-Hueckel concept in organic chemistry. Application of organic molecules and reactions. *Acc. Chem. Res.* **1971**, *4*, 272−280.
(4) Yoshizawa, K.; Tada, T.; Staykov, A. Orbital Views of the Electron Transport in Molecular Devices. *J. Am. Chem. Soc.* **2008**, *130*, 9406−9413.
(5) Krylov, A. I. From orbitals to observables and back. *J. Chem. Phys.* **2020**, *153*, 080901.
(6) Chiu, Y. N. Triplet-to-singlet cyclopropylidene-allene rearrangement. A molecular example of spin angular momentum coupling in orthogonal π systems. *J. Am. Chem. Soc.* **1982**, *104*, 6937−6942.
(7) Chiu, Y.-N. Bond-alternating Hückel-Möbius and related, twisted linear, cyclic and helical systems—their molecular orbitals, energies and phase correlation upon dissociation. *Theor. Chim. Acta* **1983**, *62*, 403−427.
(8) Becker, J. Y. Electrochemical Oxidation and Reduction of Allenes. *Isr. J. Chem.* **1985**, *26*, 196−206.
(9) Chentit, M.; Sidorenkova, H.; Jouaiti, A.; Terron, G.; Geoffroy, M.; Ellinger, Y. The structure of diphosphaallenic radical cations as evidenced by EPR experiments and ab initio calculations. *J. Chem. Soc., Perkin Trans. 2* **1997**, 921−926.
(10) Hendon, C. H.; Tiana, D.; Murray, A. T.; Carbery, D. R.; Walsh, A. Helical frontier orbitals of conjugated linear molecules. *Chem. Sci.* **2013**, *4*, 4278−4284.
(11) Thulstrup, P. W.; Hoffmann, S. V.; Hansen, B. K. V.; Spanget-Larsen, J. Unique interplay between electronic states and dihedral angle for the molecular rotor diphenyldiacetylene. *Phys. Chem. Chem. Phys.* **2011**, *13*, 16168−16174.
(12) Liu, M.; Artyukhov, V. I.; Lee, H.; Xu, F.; Yakobson, B. I. Carbyne from First Principles: Chain of C Atoms, a Nanorod or a Nanorope. *ACS Nano* **2013**, *7*, 10075−10082.
(13) Guo, Y. D.; Yan, X. H.; Xiao, Y. Conformational change-induced switching behavior in pure-carbon systems. *RSC Adv.* **2013**, *3*, 16672−16680.
(14) Imamura, A.; Aoki, Y. Helical molecular orbitals around straight-chain polyyne oligomers as models for molecular devices. *Chem. Phys. Lett.* **2013**, *590*, 136−140.
(15) Garner, M. H.; Hoffmann, R.; Rettrup, S.; Solomon, G. C. Coarctate and Möbius: The Helical Orbitals of Allene and Other Cumulenes. *ACS Cent. Sci.* **2018**, *4*, 688−700.
(16) Gückel, S.; Gluyas, J. B. G.; El-Tarhuni, S.; Sobolev, A. N.; Whiteley, M. W.; Halet, J.-F.; Lapinte, C.; Kaupp, M.; Low, P. J. Iron versus Ruthenium: Clarifying the Electronic Differences between Prototypical Mixed-Valence Organometallic Butadiyndiyl Bridged Molecular Wires. *Organometallics* **2018**, *37*, 1432−1445.
(17) Gunasekaran, S.; Venkataraman, L. Tight-binding analysis of helical states in carbyne Tight-binding analysis of helical states in carbyne. *J. Chem. Phys.* **2020**, *153*, 124304.
(18) Chiu, Y.-N. Optical Activity of Nascent Twisted Allene and its Induction by Circularly Polarized Light. *Isr. J. Chem.* **1985**, *26*, 166−173.
(19) Caricato, M. Orbital Analysis of Molecular Optical Activity Based on Configuration Rotatory Strength. *J. Chem. Theory Comput.* **2015**, *11*, 1349−1353.
(20) Tiana, D.; Hendon, C. H.; Walsh, A. Ligand design for long-range magnetic order in metal-organic frameworks. *Chem. Commun.* **2014**, *50*, 13990−13993.
(21) Peeks, M. D.; Neuhaus, P.; Anderson, H. L. Experimental and computational evaluation of the barrier to torsional rotation in a butadiyne-linked porphyrin dimer. *Phys. Chem. Chem. Phys.* **2016**, *18*, 5264−5274.
(22) Sarbadhikary, P.; Shil, S.; Panda, A.; Misra, A. A Perspective on Designing Chiral Organic Magnetic Molecules with Unusual Behavior in Magnetic Exchange Coupling. *J. Org. Chem.* **2016**, *81*, 5623−5630.
(23) Martin, W. R.; Ball, D. W. Small Organic Azides as High Energy Materials: Perazidoacetylene, -ethylene, and -allene. *ChemistrySelect* **2018**, *3*, 7222−7225.
(24) Garner, M. H.; Jensen, A.; Hyllested, L. O.; Solomon, G. C. Helical orbitals and circular currents in linear carbon wires. *Chem. Sci.* **2019**, *10*, 4598−4605.
(25) Orimoto, Y.; Aoki, Y.; Imamura, A. Extraction of One-Handed Helical Frontier Orbital in even [*n*]Cumulenes by Breaking Mirror Images of Right- and Left-Handed Helical Orbitals: Theoretical Study. *J. Phys. Chem. C* **2019**, *123*, 11134−11139.
(26) Ozcelik, A.; Aranda, D.; Gil-Guerrero, S.; Pola-Otero, X. A.; Talavera, M.; Wang, L.; Behera, S. K.; Gierschner, J.; Peña-Gallego, A.; Santoro, F.; et al. Distinct Helical Molecular Orbitals through Conformational Lock. *Chem. - Eur. J.* **2020**, *26*, 17342−17349.
(27) Garner, M. H.; Bro-Jørgensen, W.; Solomon, G. C. Three Distinct Torsion Profiles of Electronic Transmission through Linear Carbon Wires. *J. Phys. Chem. C* **2020**, *124*, 18968−18982.
(28) Garner, M. H.; Corminboeuf, C. Correlation between Optical Activity and the Helical Molecular Orbitals of Allene and Cumulenes. *Org. Lett.* **2020**, *22*, 8028−8033.
(29) Pinter, P.; Munz, D. Controlling Möbius-Type Helicity and the Excited-State Properties of Cumulenes with Carbenes. *J. Phys. Chem. A* **2020**, *124*, 10100−10110.
(30) Garner, M. H.; Corminboeuf, C. Helical electronic transitions of spiroconjugated molecules. *Chem. Commun.* **2021**, *57*, 6408−6411.
(31) Ramirez, M.; Svatunek, D.; Liu, F.; Garg, N. K.; Houk, K. N. Origins of Endo Selectivity in Diels−Alder Reactions of Cyclic Allene Dienophiles. *Angew. Chem., Int. Ed.* **2021**, *60*, 14989−14997.
(32) Sarbadhikary, P.; Misra, A. Magnetic Modulation in Heteroallene and Heterocumulene Based tert-butyl Nitroxide Diradicals: Spin Delocalization and Conformation Play Crucial Roles. *ChemPhysChem* **2021**, *22*, 1379.
(33) Baronas, P.; Komskis, R.; Tankelevičiutė, E.; Adomėnas, P.; Adomėnienė, O.; Juršėnas, S. Helical Molecular Orbitals to Induce Spin−Orbit Coupling in Oligoyne-Bridged Bifluorenes. *J. Phys. Chem. Lett.* **2021**, *12*, 6827−6833.
(34) O'Neill, B. *Elementary Differential Geometry*; Academic Press: 1966.
(35) Perdew, J. P.; Burke, K.; Ernzerhof, M. Generalized Gradient Approximation Made Simple. *Phys. Rev. Lett.* **1996**, *77*, 3865−3868.
(36) Dunning, T. H. Gaussian basis sets for use in correlated molecular calculations. I. The atoms boron through neon and hydrogen. *J. Chem. Phys.* **1989**, *90*, 1007−1023.
(37) Woon, D. E.; Dunning, T. H. Gaussian basis sets for use in correlated molecular calculations. III. The atoms aluminum through argon. *J. Chem. Phys.* **1993**, *98*, 1358−1371.
(38) Andrae, D.; Häußermann, U.; Dolg, M.; Stoll, H.; Preuß, H. Energy-adjusted ab initio pseudopotentials for the second and third row transition elements. *Theor. Chim. Acta* **1990**, *77*, 123−141.
(39) Harris, C. R.; Millman, K. J.; van der Walt, S. J.; Gommers, R.; Virtanen, P.; Cournapeau, D.; Wieser, E.; Taylor, J.; Berg, S.; Smith, N. J.; et al. Array programming with NumPy. *Nature* **2020**, *585*, 357−362.

(40) Mayerle, J. J.; Flandera, M. A. Bis(1-carbazolyl)butadiyne. *Acta Crystallogr., Sect. B: Struct. Crystallogr. Cryst. Chem.* **1978**, *34*, 1374−1376.
(41) Petrov, A. R.; Daniliuc, C. G.; Jones, P. G.; Tamm, M. A Novel Synthetic Approach to Diaminoacetylenes: Structural Characterization and Reactivity of Aromatic and Aliphatic Ynediamines. *Chem. - Eur. J.* **2010**, *16*, 11804−11808.
(42) Tokutome, Y.; Okuno, T. Preparations, crystal polymorphs and DFT calculations of N1,N1,N4,N4-tetraphenylbuta-1,3-diyne-1,4-diamine. *J. Mol. Struct.* **2013**, *1047*, 136−142.
(43) Doan, T.-H.; Talbi, I.; Lohier, J.-F.; Touil, S.; Alayrac, C.; Witulski, B. Synthesis, crystal structure, optical, electrochemical and thermal properties of the ynamide: Bis-(*N*-4-methylbenzenesulfonyl, *N*-*n*-butyl)-1,3-butadiyne-1,4-diamide. *J. Mol. Struct.* **2016**, *1116*, 127−134.
(44) Kozhemyakin, Y.; Krämer, M.; Rominger, F.; Dreuw, A.; Bunz, U. H. F. A Tethered Tolane: Twisting the Excited State. *Chem. - Eur. J.* **2018**, *24*, 15219−15222.
(45) Hoffmann, R. Extended hückel theory − v: Cumulenes, polyenes, polyacetylenes and C_n. *Tetrahedron* **1966**, *22*, 521−538.
(46) Auffrant, A.; Jaun, B.; Jarowski, P. D.; Houk, K. N.; Diederich, F. Peralkynylated Buta-1,2,3-Trienes: Exceptionally Low Rotational Barriers of Cumulenic C = C Bonds in the Range of Those of Peptide C−N Bonds. *Chem. - Eur. J.* **2004**, *10*, 2906−2911.
(47) Jarowski, P. D.; Diederich, F.; Houk, K. N. Butatrienes as Extended Alkenes: Barriers to Internal Rotation and Substitution Effects on the Stabilities of the Ground States and Transition States. *J. Phys. Chem. A* **2006**, *110*, 7237−7246.
(48) Bühringer, M. U.; Padberg, K.; Phleps, M. D.; Maid, H.; Placht, C.; Neiss, C.; Ferguson, M. J.; Görling, A.; Tykwinski, R. R. Double Bonds? Studies on the Barrier to Rotation about the Cumulenic C = C Bonds of Tetraaryl[*n*]cumulenes (n = 3, 5, 7, 9). *Angew. Chem., Int. Ed.* **2018**, *57*, 8321−8325.
(49) Zang, Y.; Zou, Q.; Fu, T.; Ng, F.; Fowler, B.; Yang, J.; Li, H.; Steigerwald, M. L.; Nuckolls, C.; Venkataraman, L. Directing isomerization reactions of cumulenes with electric fields. *Nat. Commun.* **2019**, *10*, 4482.
(50) Wendinger, D.; Tykwinski, R. R. Odd [n]Cumulenes (n = 3, 5, 7, 9): Synthesis, Characterization, and Reactivity. *Acc. Chem. Res.* **2017**, *50*, 1468−1479.
(51) Gluyas, J. B. G.; Gückel, S.; Kaupp, M.; Low, P. J. Rational Control of Conformational Distributions and Mixed-Valence Characteristics in Diruthenium Complexes. *Chem. - Eur. J.* **2016**, *22*, 16138−16146.
(52) Parthey, M.; Gluyas, J. B. G.; Schauer, P. A.; Yufit, D. S.; Howard, J. A. K.; Kaupp, M.; Low, P. J. Refining the Interpretation of Near-Infrared Band Shapes in a Polyynediyl Molecular Wire. *Chem. - Eur. J.* **2013**, *19*, 9780−9784.
(53) Sato, M.; Kubota, Y.; Kawata, Y.; Fujihara, T.; Unoura, K.; Oyama, A. Synthesis and Some Properties of Binuclear Ruthenocenes Bridged by Oligoynes: Formation of Bis(cyclopentadienylidene)-cumulene Diruthenium Complexes in the Two-Electron Oxidation. *Chem. - Eur. J.* **2006**, *12*, 2282−2292.
(54) Januszewski, J. A.; Tykwinski, R. R. Synthesis and properties of long [*n*]cumulenes ($n \geq 5$). *Chem. Soc. Rev.* **2014**, *43*, 3184−3203.
(55) Coletti, C.; Marrone, A.; Re, N. Metal complexes containing allenylidene and higher cumulenylidene ligands: a theoretical perspective. *Acc. Chem. Res.* **2012**, *45*, 139−149.
(56) Bruce, M. I. Metal complexes containing cumulenylidene ligands, $\{L_mM\}=C(=C)_n=CRR'(n \geq 2)$. *Coord. Chem. Rev.* **2004**, *248*, 1603−1625.
(57) Auger, N.; Touchard, D.; Rigaut, S.; Halet, J.-F.; Saillard, J.-Y. Electronic Structure of Ruthenium Cumulene Complexes $[Cl(PH_3)_4RuC_nH_2]^+$ (n = 1−8) and of Their Reduced States. Bonding and Properties of the Cationic, Neutral, and Anionic Series with Respect to the Cumulenic Chain Length. *Organometallics* **2003**, *22*, 1638−1644.
(58) Marrone, A.; Re, N. Effects of terminal substituants on metallacumulene complexes: A density functional study on $(Co)_5Cr(=C)_nX_2$ (X = F, SiH3, CHCH2, NH2, NO2). *Organometallics* **2002**, *21*, 3562−3571.
(59) Touchard, D.; Dixneuf, P. A new class of carbon-rich organometallics. The C_3, C_4 and C_5 metallacumulenes Ru = (C =)$_n$CR$_2$. *Coord. Chem. Rev.* **1998**, *178*−*180*, 409−429.
(60) Fischer, E. O.; Kalder, H.-J.; Frank, A.; Köhler, F. H.; Huttner, G. 3-Dimethylamino-3-phenylallenylidene, A Novel Ligand at the Pentacarbonyl-chromium and -tungsten Skeleton. *Angew. Chem., Int. Ed. Engl.* **1976**, *15*, 623−624.
(61) Berke, H. Simple Synthesis of Dicarbonyl(η-cyclopentadienyl)-(3,3-di-tert-butyl-alleny-lidene)manganese. *Angew. Chem., Int. Ed. Engl.* **1976**, *15*, 624−624a.
(62) Naher, M.; Bock, S.; Langtry, Z. M.; O'Malley, K. M.; Sobolev, A. N.; Skelton, B. W.; Korb, M.; Low, P. J. Synthesis, Structure and Physical Properties of "wire-like" Metal Complexes. *Organometallics* **2020**, *39*, 4667−4687.
(63) Hall, M. R.; Korb, M.; Moggach, S. A.; Low, P. J. Further Chemistry of Ruthenium Alkenyl Acetylide Complexes: Routes to Allenylidene Complexes via a Series of Electrophilic Addition Reactions. *Organometallics* **2020**, *39*, 2838−2853.
(64) Hansmann, M. M.; Rominger, F.; Hashmi, A. S. K. Gold−allenylidenes − an experimental and theoretical study. *Chem. Sci.* **2013**, *4*, 1552−1559.
(65) Cadierno, V.; Gimeno, J. Allenylidene and higher cumulenylidene complexes. *Chem. Rev.* **2009**, *109*, 3512−3560.
(66) Rigaut, S.; Costuas, K.; Touchard, D.; Saillard, J. Y.; Golhen, S.; Dixneuf, P. H. Bis-allenylidene Metal Complex and Unique Related Radical with Delocalization of One Electron over Both Trans Carbon-Rich Chains. *J. Am. Chem. Soc.* **2004**, *126*, 4072−4073.
(67) Bildstein, B.; Skibar, W.; Schweiger, M.; Kopacka, H.; Wurst, K. In situ synthesis of the first C7 cumulene $(Fc)_2$=C = C=C = C=C = C=C$(Fc)_2$ via deprotonation of its conjugate $[(Fc)_2C_7H(Fc)_2]^+BF_4^-$ (Fc = ferrocenyl). *J. Organomet. Chem.* **2001**, *622*, 135−142.
(68) Simmons, H. E.; Fukunaga, T. Spiroconjugation. *J. Am. Chem. Soc.* **1967**, *89*, 5208−5215.
(69) Hoffmann, R.; Imamura, A.; Zeiss, G. D. Spirarenes. *J. Am. Chem. Soc.* **1967**, *89*, 5215−5220.
(70) Dürr, H.; Gleiter, R. Spiroconjugation. *Angew. Chem., Int. Ed. Engl.* **1978**, *17*, 559−569.
(71) Billups, W. E.; Haley, M. M. Spiropentadiene. *J. Am. Chem. Soc.* **1991**, *113*, 5084−5085.
(72) Honda, S.; Sugawara, R.; Ishida, S.; Iwamoto, T. A Spiropentasiladiene Radical Cation: Spin and Positive Charge Delocalization across Two Perpendicular Si = Si Bonds and UV—vis−NIR Absorption in the IR-B Region. *J. Am. Chem. Soc.* **2021**, *143*, 2649−2653.
(73) Terada, N.; Uematsu, K.; Higuchi, R.; Tokimaru, Y.; Sato, Y.; Nakano, K.; Nozaki, K. Synthesis and Properties of Spiro-double Sila[7]helicene: The LUMO Spiro-conjugation. *Chem. - Eur. J.* **2021**, *27*, 9342−9349.
(74) Wittig, G.; Fritze, P. On the Intermediate Occurrence of 1,2-Cyclohexadiene. *Angew. Chem., Int. Ed. Engl.* **1966**, *5*, 846−846a.
(75) Daoust, K. J.; Hernandez, S. M.; Konrad, K. M.; Mackie, I. D.; Winstanley, J.; Johnson, R. P. Strain estimates for small-ring cyclic allenes and butatrienes. *J. Org. Chem.* **2006**, *71*, 5708−5714.
(76) Hopf, H.; Markopoulos, G. The chemistry of bisallenes. *Beilstein J. Org. Chem.* **2012**, *8*, 1936−1998.
(77) Barber, J. S.; Yamano, M. M.; Ramirez, M.; Darzi, E. R.; Knapp, R. R.; Liu, F.; Houk, K. N.; Garg, N. K. Diels−Alder cycloadditions of strained azacyclic allenes. *Nat. Chem.* **2018**, *10*, 953−960.
(78) Yu, S.; Vermeeren, P.; Dommelen, K.; Bickelhaupt, F. M.; Hamlin, T. A. Understanding the 1,3-Dipolar Cycloadditions of Allenes. *Chem. - Eur. J.* **2020**, *26*, 11529−11539.
(79) Anthony, S. M.; Wonilowicz, L. G.; McVeigh, M. S.; Garg, N. K. Leveraging Fleeting Strained Intermediates to Access Complex Scaffolds. *JACS Au* **2021**, *1*, 897−912.
(80) Johnson, R. P. Strained Cyclic Cumulenes. *Chem. Rev.* **1989**, *89*, 1111−1124.

https://doi.org/10.1021/acs.jpca.1c05799
J. Phys. Chem. A 2021, 125, 8107−8115